Korean J. Chem. Eng., 32(8), 1586-1597 (2015)
DOI: 10.1007/s11814-014-0380-0

pISSN: 0256-1115
eISSN: 1975-7220

On the positive role of doping Cu and N_2 on TiO_2 in improving dye degradation efficiency: Providing reaction mechanisms

Mohammad Ebrahim Olya and Azam Pirkarami†

Department of Environmental Research, Institute for Color Science and Technology, P. O. Box 16765-654, Tehran, Iran
(*Received 10 August 2014 • accepted 20 December 2014*)

Abstract−This paper reports an investigation into the effect of a number of operating factors on the removal of Ponceau 4R (Acid Red 18) from an aqueous solution through photodegradation in the presence of nitrogen. N_2 was doped in situ on Cu-TiO_2. The photocatalyst was UV/TiO_2-Cu applied in suspension to the solution to achieve a larger catalyst surface area. The optimal values of photocatalyst dose, dye concentration, and pH were found to be 0.8 mg L^{-1}, 20 mg L^{-1}, and 7, respectively. The nitrogen gas was found to have a highly positive role in degradation. The aqueous solution was characterized for its COD. Photocatalyst efficiency was evaluated using XRD, SEM, and EPR techniques. The post-treatment product was characterized using FT-IR, HPLC, and GC-MS studies, intermediate compounds were detected, and a pathway was proposed for the degradation of the dye.

Keywords: UV/TiO_2-Cu, Nitrogen Gas, Photodegradation, Ponceau 4R

INTRODUCTION

Azo dyes are an important category of synthetic organic compounds characterized by the presence of one or more azo bonds -N=N-. They represent almost 50% of dye production worldwide and are extensively used in industries such as textile, leather dyeing, cosmetics, food production, and paper printing, with the textile industry being the largest consumer [1,2], because of their chemical stability, ease of synthesis, and versatility [3]. Traditional methods for dye removal include biological treatment [4], coagulation [5], adsorption [6], flotation [7], membrane separations [8], electrochemical methods [9-11], foam flotation [12], nanofiltration [13], and biosorption [14]. However, due to high dye concentrations and the increased stability of synthetic dyes, these methods are becoming less effective for the treatment of colored industrial effluents [14,15]. Researchers have thus turned to another technique: photocatalysis (PC) [16-18]. This process generally involves subjecting a semiconductor (usually titanium dioxide nanoparticles [19,20]) used as the photocatalyst to ultraviolet (UV) irradiation. As a result, the electrons in the semiconductor are excited from the valence band to the conduction band, thus generating the electron-hole (H^+/e^-) pairs [21,22]. These photo-generated pairs produce hydroxyl radicals [23], which convert organic pollutants ad- sorbed on the surface of the photocatalyst to less harmful products [24].

Nano-sized titanium dioxide (TiO_2) has been widely utilized as a photocatalyst for the removal of contaminants such as dyes, microbiologica, organic materials, inorganic, and oils [25,26]. TiO_2 is comparatively inexpensive, non-toxic, highly stable, and environmentally friendly [27,28], and it has an appropriate band-gap (3.0 eV) to adsorb UV light at 365 nm [29].

The photoelectrocatalytic capability of TiO_2 can be enhanced by doping it with metals such as Cr, Fe, Ni, Cu, Ag, and Ti [30-34]. Doping enhances degradation by forming more hole-electron (h^+-e^-) pairs and keeping the electrons and holes separate [35-37]. Sometimes the degradation capability of doped TiO_2 is further enhanced by blowing nitrogen into the aqueous solution [38]. Since copper is relatively more abundant and less costly than other metals, it a common dopant for TiO_2 surface [39]. In particular, Cu(II) has been shown to modify the valence band spectrum [40] and improve photocatalytic activity [41-44] of TiO_2. Cu/TiO_2 has been widely used as a photocatalyst [39,45-52]. To give extended examples, [39] studied the effect of Cu/TiO_2 thin films on photocatalytic degradation of methylene blue, and [52] investigated the impact of Cu/TiO_2 on the photodegradation of dihydroxybenzenes. Furthermore, Cu/TiO_2 has been used in the treatment of gaseous pollutants [53,54], and some studies have also found that Cu/TiO_2 has considerable potential for generating hydrogen [55,56].

Lee et al. [57] proposed TiO_2/CuO as a new photocatalyst for purifying dye wastewater. They reported a reduction of 46% in the concentration of Acid Orange 7 (AO7) in wastewater in comparison with an AO7 removal of only 25% in the presence of bare TiO_2.

Nitrogen has been demonstrated to improve photocatalytic activity of TiO_2 in visible light regions [58]. For instance, [59] found that TiO_2 in N_2 atmosphere decomposes organic compound in wavelengths of up to 550 nm. Elsewhere, Cu-TiO_2 was treated with N_2 [60]. Doping N_2 onto TiO_2 has been accomplished using several methods such as sputtering [61], annealing under NH_3 [62], ion implantation [63], dip calcinations [64], hydrothermal method [65], sol-gel [66], and electrochemistry [67].

The present study was conducted to examine the impact of a number of operating parameters on the efficiency of removing Ponceau 4R (Acid Red 18) from an aqueous solution through PC, with TiO_2 doped with Copper (UV/TiO_2-Cu) as the photocatalyst in the presence of the nitrogen gas which had been doped in situ

†To whom correspondence should be addressed.
E-mail: a.pirkarami@gmail.com

on Cu-TiO_2. The parameters were photocatalyst quantity, dye concentration, pH. UV/TiO_2-Cu was applied to the solution in suspension. This suspension mode increases the photocatalyst surface area and the contact between the photocatalyst and the pollutant molecules, thus improving the efficiency of photocatalytic degradation [68]. The problem of separating the UV/TiO_2-Cu powder from the treated solution [69] was dealt with by subjecting the post-treatment solution to centrifugation. To judge the efficiency of the PC process, the COD (chemical oxygen demand) test was used. The efficiency of the photocatalyst was studied using XRD, SEM, and EPR techniques. The post-treatment product was characterized using HPLC, FT-IR, and GC-MS techniques. What is novel about this research is that, to the best of our knowledge, the effect of doping TiO_2 with Cu and N_2 on the efficiency of azo dye degradation has not been investigated in previous studies.

EXPERIMENTAL

1. Reagents

The chemicals used in this research were titanium tetraisopropoxide (TTIP), copper(II) nitrate hexahydrate, diethanolamine, glacial acetic acid, absolute alcohol, and deionized water. Deionized water was produced by the researchers. All the other chemical reagents (purchased and used as received from Merck in Germany) were of analytical grade or better quality.

2. Preparation of the Photocatalyst

The photocatalyst used in this study was TiO_2 doped with copper (UV/TiO_2-Cu). The components of the nano-sized powder were synthesized separately before they were mixed via a sol-gel process. The procedures are given below.

To prepare TiO_2, hydroxyl propyl cellulose (HPC) was dissolved in ethanol (C_2H_5OH, 99% pure product of Cympranglud B.V.), under fast stirring for 5 min. Then, titanium tetra isopropoxide (TTIP) was added, and the mixture was stirred for 20 min. The mol ratio of TTIP : HPC : ethanol must be kept at 1 : 2.33 : 10.52, (v/v) respectively. Another addition was a mixture of glacial acetic acid, absolute ethanol and deionized water in the molar ratio 10 : 8 : 100, (v/v), respectively. The pH of the solution was set at 7. This was followed by 20 minutes of stirring to ensure a yellow transparent acidic TiO_2 sol. The sol was allowed to stand for 40 min at room temperature. Glacial acetic acid was used as an inhibitor to slow down the TTIP hydrolysis. The copper sol was prepared as follows. First, copper(II) nitrate hexahydrate was dissolved in absolute alcohol and was stirred for 10 min. Then, a mixture of diethanolamine, absolute alcohol, and deionized water, (4 : 10 : 74 volumetric ratio) was poured into the solution under fast stirring. The resulting solution was continuously stirred for 20 min to achieve a transparent alkaline copper sol.

For the final UV/TiO_2-Cu photocatalyst, the Cu sol was directly added into the TiO_2 sol. The resultant nanocomposite was allowed to dry at room temperature. Then, it was calcined at 360 °C for 15 min and subsequently at 550 °C for 5 hours, with the temperature being increased at a speed of 5 °C/Sec. Lastly, the specimen was cooled before use.

3. Materials and Equipment

The solution was prepared by pouring Ponceau 4R (Acid Red 18), obtained from the Iranian company of Alvan Sabet, into doubly distilled water. NaOH and HCl (Merck, Germany) were used to adjust the pH of the solution. The photocatalytic (PC) reactor was a glass container (80×70×290 mm), with its walls covered with aluminum foil. The excitation source was a 6 W UV lamp (irradiation at 365 nm) purchased from the Dutch supplier of Philips. The lamp was placed inside a single-walled quartz tube in the middle of the reactor. The efficient volume of the PC reactor was 1,000 mL after subtracting the volume occupied by the quartz tube. The sketch diagram of the reactor used in the experiment is shown in Fig. 1. To analyze the aqueous solution, COD levels were measured using a Hach spectrophotometer (Diar 5000, USA).

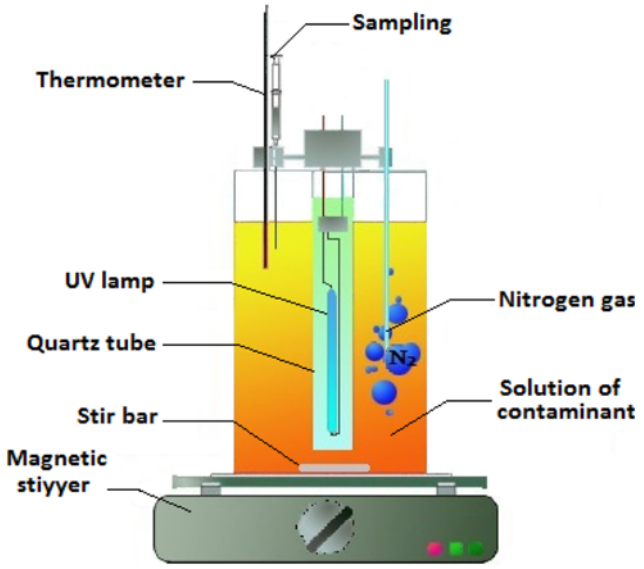

Fig. 1. Schematic representation of the of the side view of the PC reactor.

4. Procedure

The aqueous solution was prepared by dissolving dye into pure water. The pH of the solution was adjusted using NaOH and HCl. The solution was poured into the reactor and magnetically stirred at 200 rpm to ensure homogeneity. Then, the UV lamp was placed inside the reactor. N_2 (99.99%) was introduced into the reactor. All the experiments were performed under total N_2 environment. The solution was subjected to the PC process for 120 min to examine the effect of a number of operating parameters on the efficiency of removing dye from the experimental solution: photocatalyst dose, dye concentration, and pH. The effect of photocatalyst quantity was studied by applying five quantities of 0, 0.2, 0.4, 0.6, 0.8, and 1 mg L^{-1}. To determine the effect of dye concentration, six doses were considered: 10, 20, 30, 50, 80, and 100 mg L^{-1}. The impact of pH was explored by setting the pH of the solution at five values: acidic (pH 2, 5, 6), neutral (pH 7), and basic (pH 8, 9, 11). The viability of the removal technique was judged by subjecting the treated solution to COD measurement.

5. Photocatalyst Characterization

The morphological features and surface characteristics of the Cu-TiO_2 photocatalyst were studied using a scanning electron microscope (SEM) unit (HITACHI-3000 SH Model, Japan). Further, the

efficiency of the nanocomposite was evaluated through X-ray diffraction (XRD) using a Philips PW 1710 high power diffractometer (the Netherlands) with Cu Kα radiation at 40 kV and 40 mA. Finally, electron paramagnetic resonance (EPR) spectroscopy was employed to study the structure of TiO_2 and Cu-TiO_2. EPR spectra were obtained on a Bruker Elexys E580 spectrometer equipped with a helium cryostat.

6. Evaluation of Photocatalysis Efficiency

The UV absorbance of the dye was tested using a UV-visible spectrophotometer (Camspec M-350 Double Beam, UK) at a wavelength of 507 nm (the maximum absorbance wavelength of Ponceau 4R). Since the λ_{max} of the solution (507 nm) was obtained using a double beam spectrophotometer, all the results were checked using the same spectrophotometer and the same results were achieved. Five-mL samples were taken out from the solution at five-minute intervals, were subjected to centrifugation at 12,000 rpm for 10 min, and were put inside the spectrophotometer. The linear relationship between dye concentration and dye removal efficiency was determined through Eq. (1):

$$R(\%) = \frac{A - A_0}{A_0} \times 100 \quad (1)$$

where A_0 and A are the light absorbance of the dye before and after PC, respectively.

The post-treatment product was characterized using HPLC, FT-IR, and GC-MS techniques. Chromatographic analysis was performed using a high-performance liquid chromatograph (HPLC, Knauer, Germany) coupled with a UV 2600 diode-array detector (DAD) and a Smart Line 1000 pump. The separation column was ODS-C18 (5 pm, 4.6 mm×250 mm) having a precolumn of the same material, 1 cm long. A mixture of acetonitrile and water, 60 : 40 (v/v), was used as the mobile phase at a flow rate of 0.7 mL min^{-1} at room temperature. For photolysis, aliquots of approximately 2 mL were taken out at given time intervals during decolorization: 0 (before treatment), 30, 60, 90, and 120 min. Standard dye (30 mg L^{-1}) was separately injected to the HPLC device to determine its retention time.

The centrifuged samples were allowed to dry at room temperature. Then, they were mixed with spectroscopically pure KBr in the ratio of 2 : 100 to make pellets to be placed in the Shimadzu 8300 FT-IR (Perkin-Elmer, Spectrum one). FT-IR spectra were obtained in the range of 500 to 3,500 cm^{-1} for the intact dye and biodegraded dye.

The degradation products were also analyzed through gas chromatography-mass spectrometry (GC-MS) using an Agilent 7890 GC device (Agilent Technologies, USA) with a 30 m×0.25 mm HP-5MS capillary column equipped with an Agilent 5973 mass spectrometer operating in the electron mode at 70 eV. The temperature program of the column was as follows: 50 °C for 5 min, up to 300 °C at a rate of 10 °C min^{-1}. The temperature of the inlet and detector was 250 and 150 °C, respectively. Pure helium (99.999%) was used as the carrier gas at a flow rate of 1 mL min^{-1}. The intermediates formed during the photocatalytic process were compared with commercial standards, and their fragment ions in the mass spectra were interpreted under the following conditions: an m/z scan from 40 to 250, scan speed of 2000, interval of 0.5 s, and ion source temperature of 200 °C.

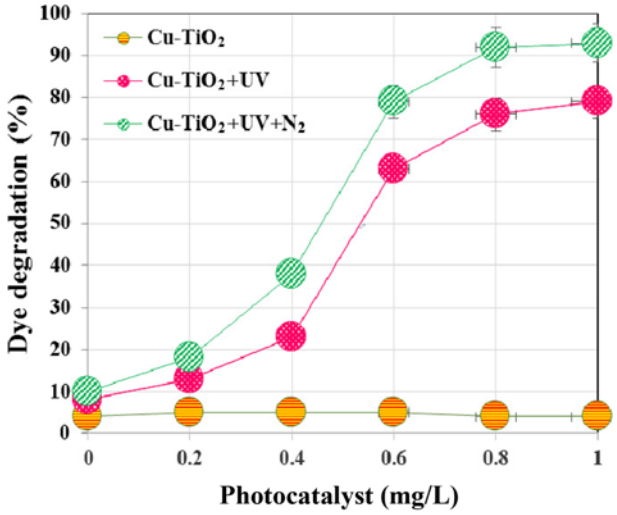

Fig. 2. Effect of photocatalyst (Cu-TiO_2) dose on the degradation of Ponceau 4R (contact time: 120 min, dye concentration: 20 mg L^{-1}, pH: 7).

RESULTS AND DISCUSSION

The photocatalytic removal of Ponceau 4R from the aqueous solution was studied at λ_{max} 507 nm. The optimal conditions for dye degradation turned out to be photocatalyst dose of 0.8 mg L^{-1}, initial dye concentration of 20 mg L^{-1}, and pH of 7. These parameters are discussed below.

1. Effect of Photocatalyst Dose

The effect of photocatalyst on the degradation of Ponceau 4R was investigated by applying five doses of nano-sized UV/TiO_2-Cu: 0, 0.2, 0.4, 0.6, 0.8, and 1 mg L^{-1}. The observation was that the PC degradation of the azo dye increased as the quantity of the nanocomposite increased. However, as Fig. 2 shows, the last two values lead to essentially the same degree of removal efficiency. As a result of this and for economic considerations, 0.8 mg L^{-1} was taken to be the optimum quantity for efficient degradation of Ponceau 4R.

Before dealing with the reaction mechanism, a discussion of the role of nitrogen in improving photocatalytic activity of NO_2 seems necessary here. Our observation seems to be consistent with previous studies which confirm that N_2 gas creates oxygen vacancies and that, as N_2 concentration in the aqueous solution increases, more nitrogen ions combine with oxygen ions [70,71]. These nitrogen-oxygen compounds cause an increase in the number of active sites in the presence of UV light and photocatalyst.

The impact of photocatalyst dose can be explained as follows. On the one hand, an increase in the amount of photocatalyst leads to a corresponding increase in the population of the photo-generated e^-/h^+ pairs and in the number of active sites ($OH^•$ and $O_2^•$ radicals) on the Cu-TiO_2 surface [72,73]. On the other hand, N_2 in the solution reacts with O_2 to form NO_2^- (Eq. (2)).

$$N_2 + 2O_2 \rightarrow 2NO_2^- \quad (2)$$

Now, the $^•OH$ and $^•O_2$ radicals oxidize NO_2^- ions into NO_3^- ions.

The reaction is given in Eq. (3) below.

$$2NO_2^- + O_2 \rightarrow 2NO_3^- \quad (3)$$

Also, the $^{\bullet}OH$ radicals attack NO_2 [74,75] and transform it to $^{\bullet}HNO_3$ or its conjugate base $(^{\bullet}NO_3)_2^-$ (Eq. (4)).

$$2NO_2^- + {}^{*}OH \rightarrow {}^{*}HNO_3^- \leftrightarrow ({}^{*}NO_3)^{2-} + H^+ \quad (4)$$

Then, both species break down to $^{\bullet}NO_2^-$ as shown by Eq. (5) and Eq. (6) below:

$${}^{*}HNO_3^- \rightarrow {}^{*}NO_2 + OH^- \quad (5)$$

$$({}^{*}NO_3)^{2-} + H_2O \rightarrow {}^{*}NO_2 + 2OH^- \quad (6)$$

$^{\bullet}NO_2$ can also exist in the solution as N_2O_4 (Eq. (7)). This dimer quickly becomes disproportionate and changes to nitrite (NO_2^-) and nitrate (NO_3^-), as shown by Eq. (8).

$$2{}^{*}NO_2 \rightarrow N_2O_4 \quad (7)$$

$$N_2O_4 + H_2O \rightarrow NO_3^- + NO_2^- + 2H^+ \quad (8)$$

$^{\bullet}OH$ quickly attacks NO_2^-, thus peroxynitrous acid (Eq. (9)), which can isomerize to nitrate (Eq. (10)).

$${}^{*}NO_2 + {}^{*}OH \rightarrow HO_2NO \quad (9)$$

$$HO_2NO \rightarrow NO_3^- + H^+ \quad (10)$$

$(^{\bullet}NO_3)^{2-}$ can be oxidized by molecular oxygen to change into nitrate and $^{\bullet}O_2^-$ radical (Eq. (11)).

$$({}^{*}NO_3)^{2-} + O_2 \rightarrow NO_3^- + {}^{*}O_2^- \quad (11)$$

To see whether dye removal is a result of dye being adsorbed onto catalyst surface or degradation owing to the presence of UV light and N_2, the following experiment was performed: Cu-TiO_2 was applied to the aqueous solution in the absence of UV light and N_2. A dye removal of only about 4% was observed. A comparison between this value and the values obtained from the other two conditions already studied (i.e., "Cu-TiO_2+UV" and "Cu-TiO_2+UV+N_2") clearly shows that dye removal is largely due to the presence of UV light and N_2.

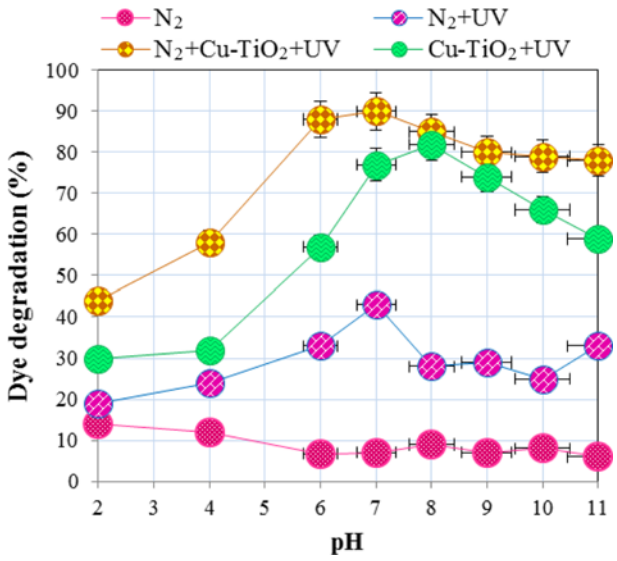

Fig. 3. Effect of initial pH value on the degradation of Ponceau 4R (contact time: 120 min, photocatalyst dose: 0.8 mg L^{-1}, dye concentration: 20 mg L^{-1}).

2. Effect of pH

Fig. 3 depicts the effect of different values of pH on the efficiency of the removal of Ponceau 4R: acidic (pH 2, 3, 5), neutral (pH 7), and basic (pH 8, 9, 11). Around 77%, 90%, and 98% of the dye had been degraded after 120 minutes of the PC process at pH values of 3, 5, and 7, respectively. This phenomenon is attributable to the fact that with an increase in the value of pH, the concentration of OH ions increases, and this leads to the generation of $OH^{\bullet}$ and $O_2^{\bullet}$

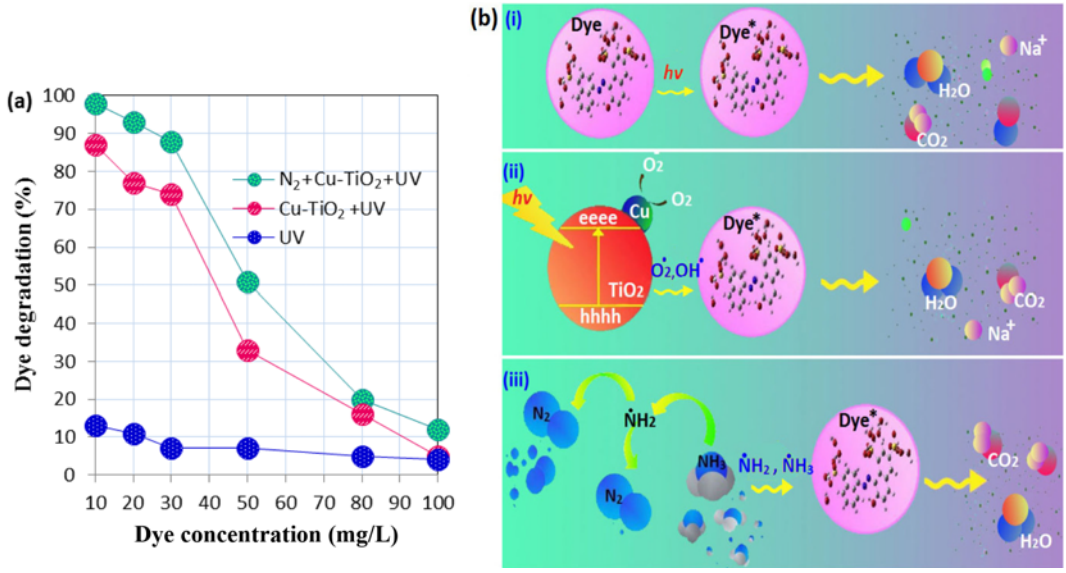

Fig. 4. (a) Effect of initial dye concentration on the degradation of Ponceau 4R (contact time: 120 min, photocatalyst dose: 0.8 mg L^{-1}, pH: 7) and (b) the stages of dye degradation.

by Cu-TiO_2. However, the rate of removal was lower for the values beyond pH 7. An explanation is that at higher pH values, the negatively charged photocatalyst surface repulses the dye anions and reduces PC efficiency [76,77]. Also, at acidic pH levels, the hydrogen atoms in the aqueous solution react with NO_2^- and NO_3^- and transforms them to $^{\bullet}NH_2^-$ and $^{\bullet}NH_3^-$, respectively. This increases the active sites in the solution which are responsible for the degradation of the dye molecules [74,75].

3. Effect of Initial Dye Concentration

To study the effect of the initial concentration of the dye on the degradation efficiency, six quantities of 10, 20, 30, 50, 80, and 100 mg L^{-1} were employed. Fig. 4 shows that changing the initial concentration from 10 to 30 mg L^{-1} resulted in a dye removal of around 97% after 120 min of PC. Also, at concentrations beyond 30 mg L^{-1} degradation rate decreased. A possible explanation is that an increase in the amount of dye in the solution prevents light photons from penetrating into the surface of the photocatalyst. In consequence, fewer hydroxyl and superoxide radicals which are capable of attacking dye molecules are formed in the reactor, and thus removal efficiency declines [78,79].

Dye degradation takes place in three stages. First, upon UV illumination, the dye electrons are excited from the valence band (VB) to the conduction band (CB). This is stage (i) in Fig. 4(b) and Eq. (12) below [73].

$$Dye_{(ads)} \xrightarrow{h\nu} {}^{*}Dye_{(ads)} \tag{12}$$

At stage (ii), H_2O_2 generated in the aqueous solution as a result of PC reactions increases the number of hydroxyl and superoxide radicals responsible for attacking the dye molecules (Eq. (13) and (14) [80].

$$H_2O_2 + h^+_{VB} \rightarrow OH_2^* + H^+ \tag{13}$$

$$OH^* + OH_2^* \rightarrow H_2O + O_2 \tag{14}$$

Finally, at stage (iii), with the addition of nitrogen to the aqueous solution, the active sites of $^{\bullet}NH_2^-$, $^{\bullet}NH_3^-$, and $^{\bullet}NO_2^-$ are generated (already discussed in Eq. (2) through Eq. (11) above).

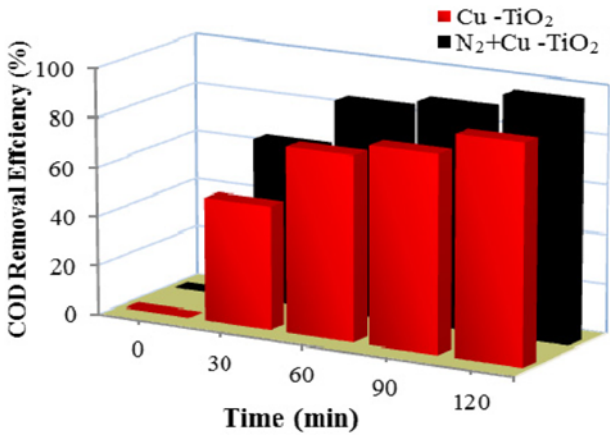

Fig. 5. The efficiencies of COD removal from the aqueous solution (photocatalyst dose: 0.8 mg L^{-1}, dye concentration: 20 mg L^{-1}, pH: 7).

4. Aqueous Solution Analysis

The COD test is widely used to judge the efficiency of dye degradation techniques by measuring the total quantity of oxygen needed for the oxidation of organic material to CO_2 and water [54,73]. In the present work, the aqueous solution was subjected to COD determination at different intervals under the optimum conditions obtained (contact time: 120 minutes, photocatalyst dose: 0.8 mg L^{-1}, pH: 7; dye concentration: 20 mg L^{-1}). Fig. 5 presents the results. The COD values decreased at an increasing rate as the PC process continued. More specifically, maximum reduction in COD values was obtained after 120 minutes of treatment: 88% for UV/TiO_2-Cu and 97% for N_2+Cu-TiO_2. This can be attributed to the degradation of complex molecules and intermediates into simple organic materials.

CHARACTERIZATION AND ANALYSIS

1. Characterization of Photocatalyst: XRD and SEM Analyses

The crystallinity of TiO_2 and Cu-TiO_2 was verified using the X-ray diffraction (XRD) technique. The crystallite sizes were calculated using the Scherrer equation [81], a formula which relates the size of crystallites in the form of powder to the broadening of a peak in a diffraction pattern. The Scherrer equation can be written as Eq. (15) below:

$$\phi = \frac{K\lambda}{\beta \cdot \cos\theta} \tag{15}$$

where Φ is the crystallite size, K a dimensionless shape factor, with its value usually taken as 0.89, λ is the X-ray wavelength, 0.154 nm, β is the peak broadening at half the maximum intensity, after subtracting the instrumental peak broadening, in radians, and θ is the diffraction angle of the anatase peak (1 0 1). The average crystallite sizes were found to be 299:68 Å=29:988 nm (TiO_2) and 254:5 Å= 25:46 nm (Cu-TiO_2).

XRD measurements were carried out in the range of $2(\theta)$=10-80°. The results are given in Fig. 6. The major diffraction peaks detected for the modified Cu-TiO_2 and unmodified TiO_2 samples appeared to be the same, but the intensities of the peaks underwent a significant reduction in the case of UV/TiO_2-Cu. In addition, peak broadening was confirmed, which might be relevant to grain refinement resulting from doping. It is believed that part of Cu that penetrated into TiO_2, and Cu ions were distributed uniformly in the interstices of semiconductor crystalline structure. Finally, no mixed phase was observed between Cu and Oxygen, a phenomenon which may be due to the low Cu loading (2%) [82].

The surface textures of undoped TiO_2 and Cu-doped TiO_2 (both before and after PC) were analyzed using the SEM technique. Fig. 6(b) shows that undoped TiO_2 surface was rough and it was composed of compactly aggregated nanoparticles. Fig. 6(c) shows that doping resulted in an increase in the surface roughness and porosity of the photocatalyst. Moreover, it was confirmed that the micropores had amorphous edges. Finally, the blocked pores seen in Fig. 6(d) confirm that the dye molecules were adsorbed on to the surface of Cu-TiO_2 during PC.

2. EPR Spectroscopy

Although XRD examination revealed the structural changes of

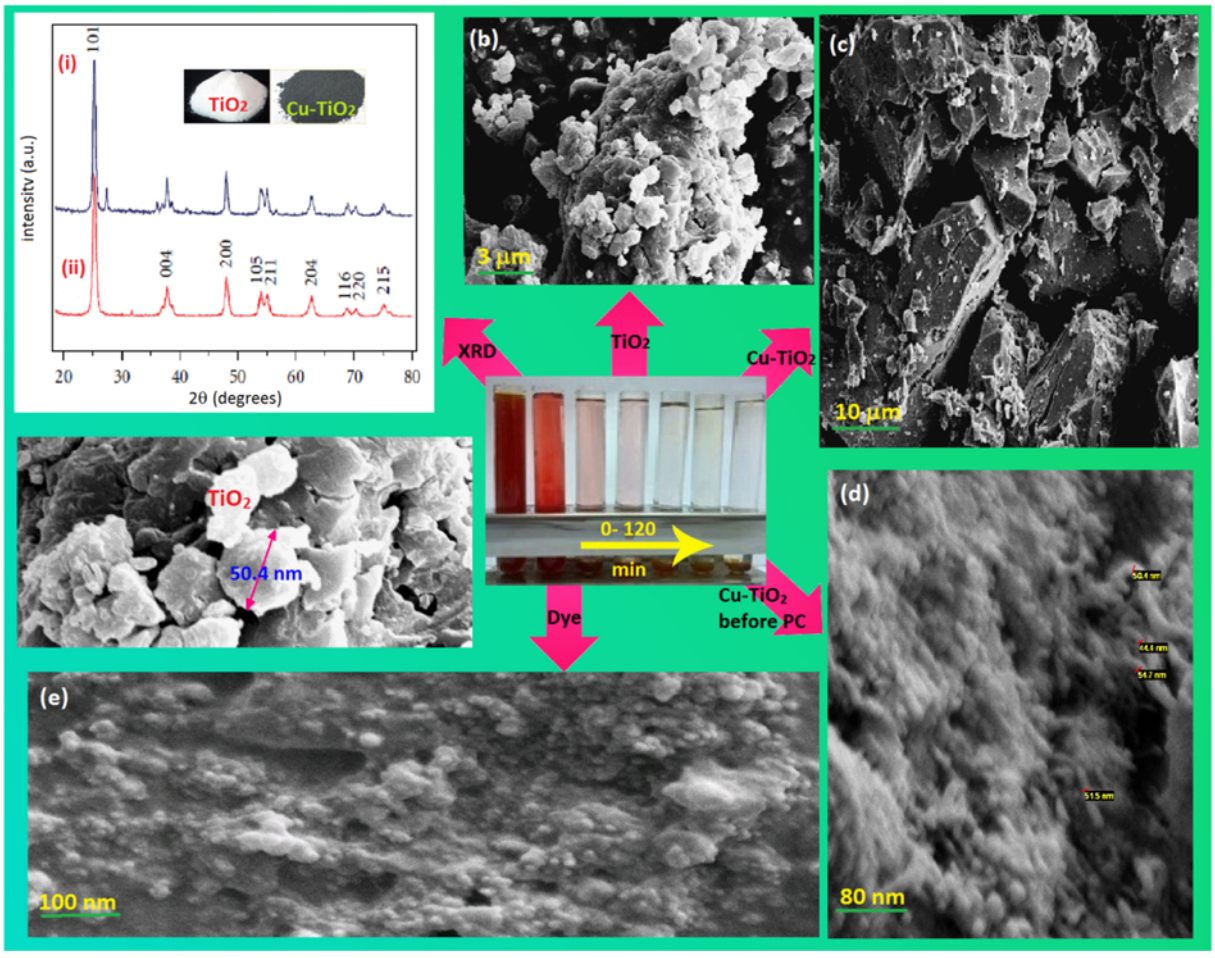

Fig. 6. (a) XRD patterns of TiO_2 (i) and Cu-TiO_2 (ii); SEM photograph of undoped TiO_2 (b), Cu-TiO_2 before PC (c), Cu-TiO_2 dyed by Ponceau 4R (d), and enlargement of part of d (e).

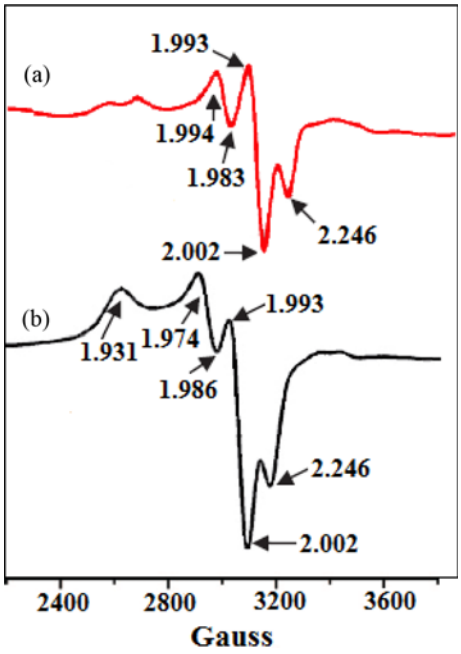

Fig. 7. EPR spectra of (a) TiO_2 and (b) Cu-TiO_2.

Cu-TiO_2 nanoparticles, it could not provide any information about Cu. Thus, we employed the EPR technique to characterize the Cu-TiO_2 photocatalyst. The EPR spectra of TiO_2 and Cu-TiO_2 nanocomposites are given in Fig. 7, indicates the presence of various paramagnetic species. In both samples, a prominent signal at g=2.002 is responsible for the maximum signal area and is possibly a result of the presence of free electrons in the conduction band [83]. G-values between 1.93 and 1.98 are due to Ti^{3+} species [84,85], and the g=2.24 signal may be due to an Cu^{2+} ions species, [85,86]. The former species acts as an electron trap, whereas the latter species acts as a photon trap [87].

3. UV-visible Photospectrometry

Dye removal measured by the UV-visible photospectrometry confirmed that the visible band at 507 nm had disappeared. Fig. 8 compares the UV-visible spectra of Ponceau 4R in the aqueous solution before and after PC. Absorbance bands in the visible region 507 nm can be attributed to the n–π* transition of the -N=N- group. The $\pi-\pi$* transition of electrons in the azo dye connecting naphthalene rings is responsible for the band in the near-ultraviolet region; the absorbance band results from the unsaturated character of the rings. The disappearance of the visible band indicates the effective destruction of the -N=N- group and the removal of the dye mole-

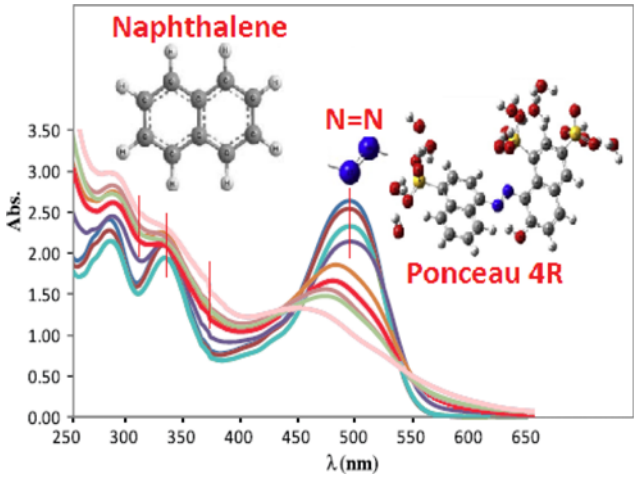

Fig. 8. The UV-visible spectra of Ponceau 4R (contact time: 120 min, photocatalyst dose: 0.8 mg L^{-1}, dye concentration: 20 mg L^{-1}, pH: 7).

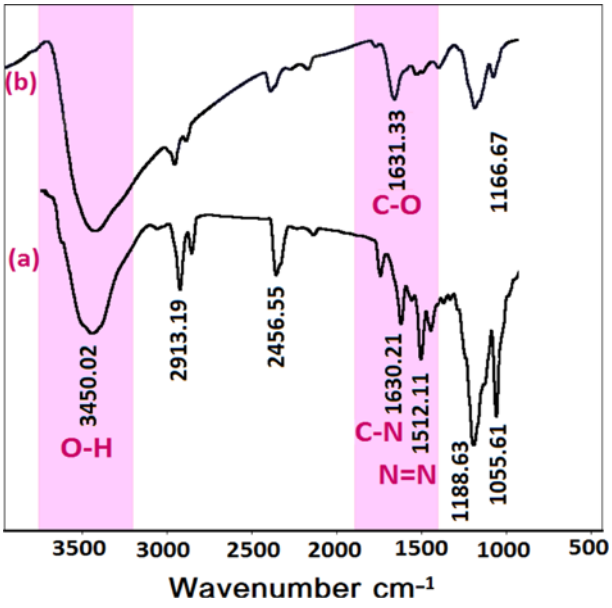

Fig. 10. The FT-IR spectra of Ponceau 4R before PC (a) and after 100 min of PC (b) (photocatalyst dose: 0.8 mg L^{-1}, dye concentration: 20 mg L^{-1}, pH: 7).

cule in the PC process. Moreover, the spectra of the initial dye concentration show UV band characteristic of -N=N- groups (507 nm) related to the naphthalene rings bonded to the -N=N- groups (290, 322, and 370 nm). This indicates that the concentration of the naphthalene rings goes into a decline as the PC process continues.

4. HPLC Analysis

To gain a better understanding of the photodegradation of Ponceau 4R, HPLC analysis was performed. Fig. 9 depicts the chromatographic behavior of the dye solution at several reaction time periods under the optimum experimental conditions obtained above. Upon injection of the initial solution, a well-developed peak appeared at the retention time of 3.5 min. However, for the aliquots taken at longer reaction times, two peaks emerged, which indicates the decomposition of the dye and the concomitant formation of a group of intermediates. Although the peak pertinent to the intermediates emerged after 10 min of treatment, these intermediates began to form with the start of the PC process. The chromatogram additionally reveals that the concentration of these compounds was insignificant after 60 min of treatment.

5. FT-IR Spectral Analysis

The efficiency of the PC treatment can be determined using the FT-IR analysis of Ponceau 4R (Fig. 10). Clearly, some structural changes took place during the PC process. In spectrum (a), the broad peak at 3,550 cm^{-1} is an indication that the O-H stretching exists. The peak at 1,630 cm^{-1} is an indicator of the combination of the carbon of the naphthalene ring with the nitrogen (i.e., the C=N group). Furthermore, the peak at 1,055 cm^{-1} indicates the existence of a large number of hydroxyl groups and intermolecular hydrogen (C-OH) bonds [88]. The intense peak at 1,512 cm^{-1} indicates an -N=N- group, and the peaks at 2,456 cm^{-1} and 2,913 cm^{-1} could be attributed to C-H stretching vibration [89]. As spectrum (b) shows, the peak of 3,550 cm^{-1} broadened after the treatment, a fact which

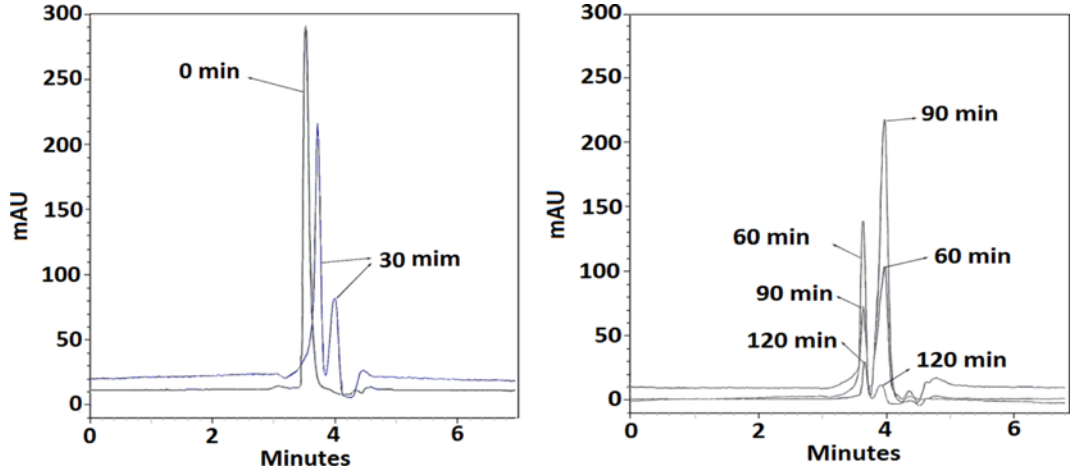

Fig. 9. The HPLC chromatogram of Ponceau 4R subjected to PC (photocatalyst dose: 0.8 mg L^{-1}, dye concentration: 20 mg L^{-1}, pH: 7).

can be attributed to the adsorption of water by the dye molecule. The other two observations from spectrum (b) are the reduction in the height of peak (b) and the complete disappearance of peaks of 1,630 cm^{-1} and 1,512 cm^{-1}. Concurrently, a new peak emerged at 1,631 cm^{-1}, suggesting the formation of the C=O group. Moreover, the peaks of 1,166 cm^{-1} in spectrum (b) and 1,188 cm^{-1} in spectrum (a) indicate C=C stretching vibration of aromatic ring [90]. These changes confirm the degradation of the organic compound and the formation of intermediate organic compounds during the PC process.

6. Photodegradation Mechanism

A mechanism can be proposed for the photodegradation of Ponceau 4R (Fig. 11). First, upon UV illumination, the electrons on Cu-TiO_2 surface are excited from the valence band (VB) to the conduction band (CB) and as a result generate electron-hole pairs (Eq. (16) and (17) below and reactions (1) and (2) in the figure) [82,92].

$$\text{Cu-TiO}_2 \xrightarrow{h\nu} \text{Cu-TiO}_2(e^-_{CB}) + \text{Cu-TiO}_2 h^+_{VB} \quad (16)$$

$$\text{Cu}_{surf}(e) + \text{Cu-TiO}_2(e^-_{CB}) + \text{reduction reaction} \quad (17)$$

Furthermore, as Eq. (18) and reaction (3) show, the copper particles doped on the surface of TiO_2 may act as electron-trapping agents and hamper the recombination of photo-generated electrons and holes. In the meantime, H_2O_2 generated as a result of reactions in the aqueous solution may expedite the process of dye degradation by increasing the number of hydroxyl and superoxide radicals responsible for attacking the dye molecules (Eq. (19) to (22) below) [93].

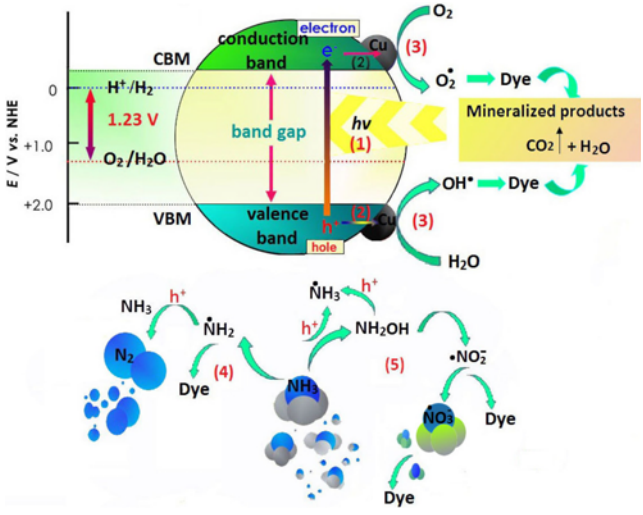

Fig. 11. Proposed mechanism for the photodegradation process in the presence of nitrogen.

$$\text{Cu}_{Surf} + \text{Cu-TiO}_2(e) \rightarrow \text{Cu}_{Surf}(e) + \text{Cu-TiO}_2 \quad (18)$$

$$H_2O_2 + \text{Cu-TiO}_2(e) \rightarrow {}^{*}OH + {}^{*}OH^- \quad (19)$$

$$H_2O_2 + h^+_{VB} \rightarrow {}^{*}OH_2 + {}^{*}H \quad (20)$$

$${}^{*}OH + OH^{*}_2 \rightarrow H_2O + O_2 \quad (21)$$

$${}^{*}OH + {}^{*}O_2 + \text{Dye} \rightarrow \text{mineral products} \quad (22)$$

On the other hand, N_2 in the solution reacts with H_2 to form NH_2 (Eq. (23) and reaction (4)).

$$N_2 + 2H_2 \rightarrow 2NH_2 \quad (23)$$

Now, as Eq. (3) below shows, the $^{\bullet}OH$ radicals oxidize NH_2 ions into NH_3 ions.

$$2NH_2 + H_2 \rightarrow 2NH_3 \quad (24)$$

In addition, $^{\bullet}NH_2$ can take the form of N_2H_4 in the solution (Eq. (25)). This dimer quickly goes out of proportion and changes to nitrite (NH_2) and nitrate (NH_3) (Eq. (26)).

$$2\,{}^{*}NH_2 \rightarrow N_2H_4 \quad (25)$$

$$N_2H_4 + H_2O \rightarrow NH_3^- + NH_2^- + 2O^- \quad (26)$$

$^{\bullet}OH$ attacks NH_2 and forms HO_2NH (Eq. (27)), which is then isomerized to nitrate (Eq. (28)).

$${}^{*}NH_2 + {}^{*}OH \rightarrow HO_2NH \quad (27)$$

$$HO_2NH \rightarrow NH_3 + O^- \quad (28)$$

$^{\bullet}NH_3$ can be oxidized by hydrogen and change to become nitrate and $^{\bullet}H_2$ radical (Eq. (29)).

$${}^{*}NH_3 + H_2 \rightarrow NH_3 + {}^{*}H_2 \quad (29)$$

Eventually, these active molecules react with the dye molecules and transform them into mineral products.

$$^{\bullet}NH_3 + {}^{\bullet}NH_2 + \text{Dye} \rightarrow \text{mineral products} \quad (30)$$

The last stage in the mechanism is reaction (5) which has already

Fig. 12. GC-MS representation of the photodegradation of Ponceau 4R.

been described in Eqs. (2) to (11).

7. GC-MS Analysis

To identify the intermediate products generated during the photodegradation of Ponceau 4R, GC-MS analysis was performed. Fig. 12 is the GC-MS representation of this process. It can be seen that the electrons generated during the treatment attack and break the C-N bond under the experimental conditions (Cu-TiO_2+N_2+hv), thus causing Ponceau 4R to degrade.

The main intermediates detected at each step of the pathway for Ponceau 4R photodegradation are given below.

The mechanism of photodegradation of Cu-TiO_2 in the presence of N_2 can be summarized as follows. First, the photocatalyst generates e^-/h^+ pairs on its surface, which in turn generate active sites ($OH^•$ and $O^•_2$ radicals) on the Cu-TiO_2 surface. At the same time, N_2 reacts with O_2 to form NO_2^-. Then, the $^•OH$ and $^•O_2$ radicals oxidize NO_2^- ions into NO_3^- ions. Subsequently, NO_3^- ions break down to $^•NO_2^-$, which then quickly changes to NO_2^- and NO_3^-. $^•OH$ attacks nitrite to form peroxynitrous acid which can isomerize to

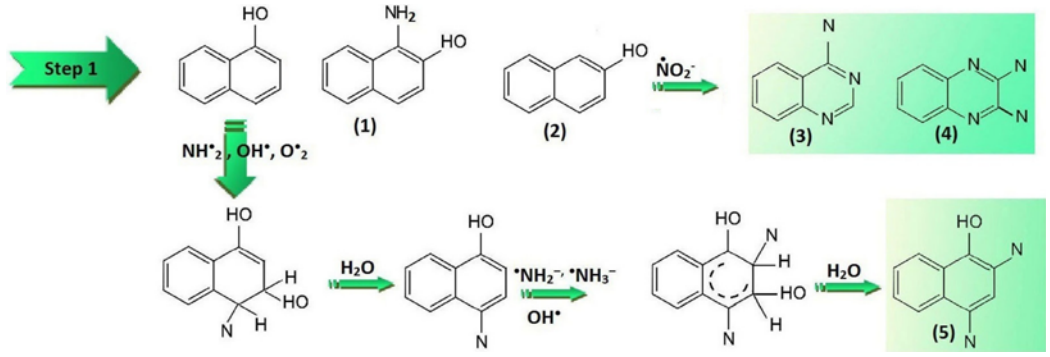

Step 1: 1-Amino-2-hydroxynaphthalene (1), Naphthalen-2-ol (2), 4-nitroquinazoline (3), 2, 3-nitroquinoxaline (4), 2,4-dinitro-1-naphthalenol (5).

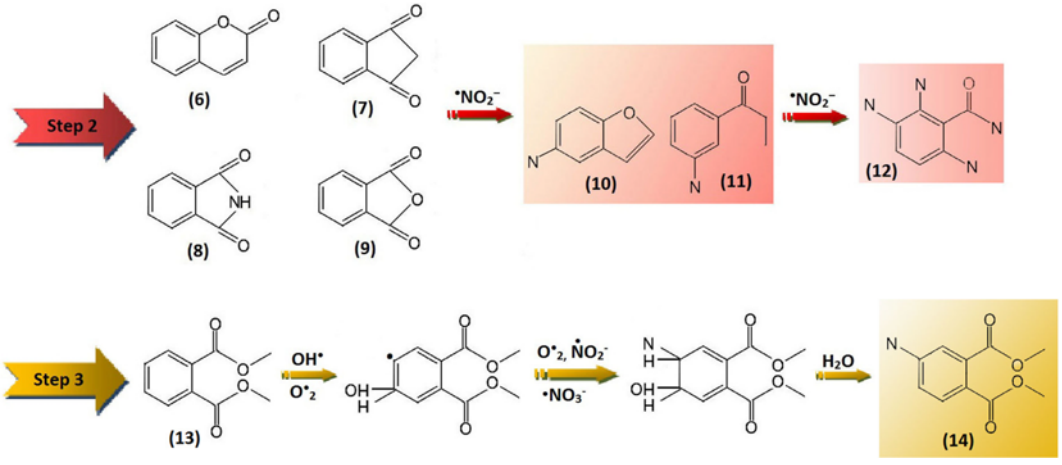

Steps 2 and 3: Coumarin (6), phthalide (7), phthalimide (8), phthalic anhydride (9), 5-nitrobenzofuranm (10), 3-nitropropiophenone (11), 2, 3, 6-trinitrobenzoyl nitride (12), dimethyl phthalate (13), dimethyl 4-nitrophthalate (14).

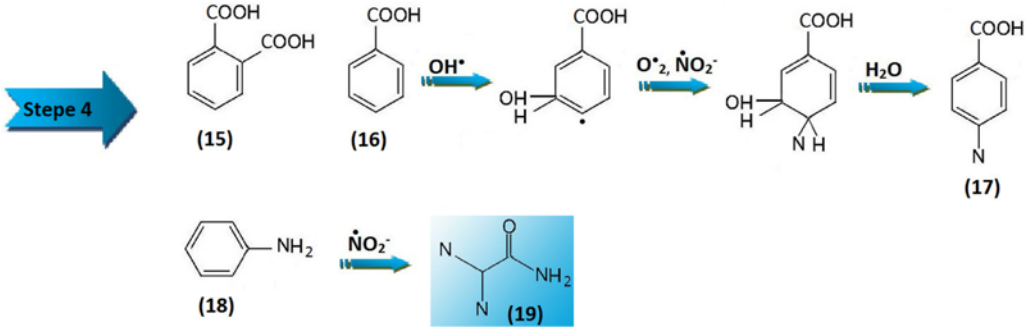

Step 4: Phthalic acid (15), benzoic acid (16), 4-nitrobenzoic acid (17), amino benzene (18) 2,2-dinitroacetamide (19).

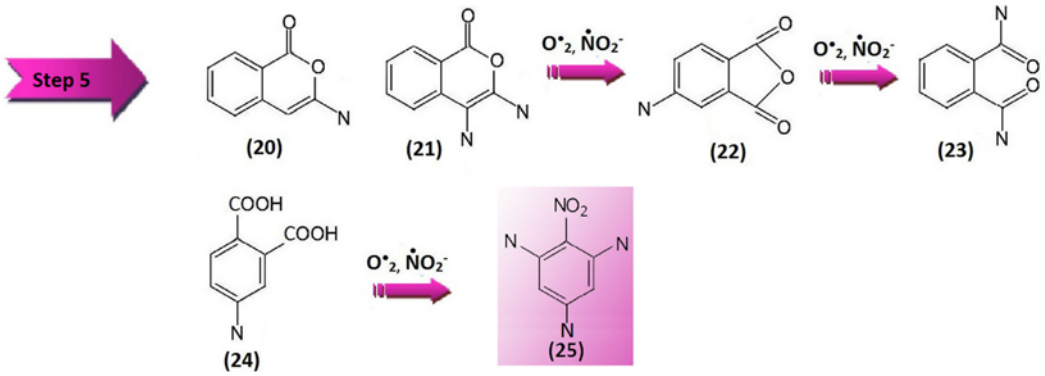

Step 5: 3-Nitroisocoumarin (20), 3,4-dinitroisocoumain (21), 5-nitroisobenzofuran-1,3-dione (22) 1,2-benzenedicarbonyl dinitride (23), 1,4-dinitrobenzene (24), 1,3,5-trinitro-2-nitrobenzene (25).

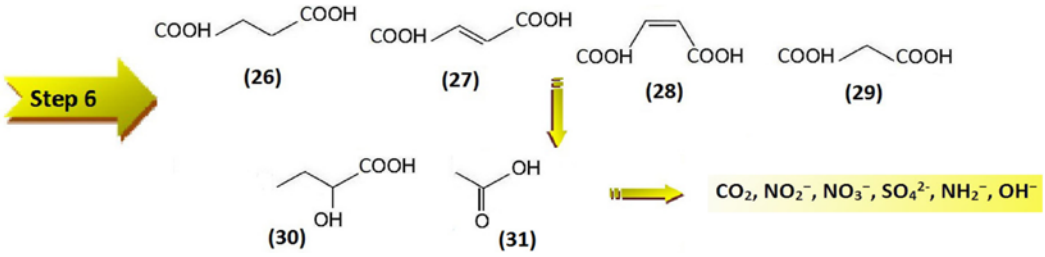

Step 6: Succinic acid (26), fumaric acid (27), maleic acid (28), malonic acid (29), 2-hydroxy butanoic acid (30), 2-hydroxy propanoic acid (31).

nitrate. ($^{\bullet}NO_3)^{2-}$ can be oxidized into nitrate and $^{\bullet}O_2^-$ radical. These radicals attacked the dye, resulting in the breakdown of dye bonds and the transformation of the dye into intermediates. Previous research [73] has shown that in some cases these intermediate compounds are even more hazardous to the environment than is the dye. However, if the duration of the reaction is extended, intermediates decompose into environmentally-friendly minerals such as CO_2 and OH.

CONCLUSION

This study aimed to optimize the photodegradation of an azo dye, Ponceau 4R, using Cu-TiO_2 as the photocatalyst applied to the aqueous solution in suspension and in the presence of the nitrogen gas doped in situ on Cu-TiO_2. The operational parameters were photocatalyst dose, dye concentration, and pH. The optimum nanocomposite dose for efficient dye degradation was found to be 0.8 mg L^{-1}. It was also observed that a value of 20 mg L^{-1} for initial dye concentration causes maximum removal (97%). However, the rate of degradation decreased at higher concentrations. Furthermore, a pH value of 7 led to the highest efficiency of photodegradation. In addition, a very influential role was observed for nitrogen in the degradation process. Another observation was the substantial reduction in the COD values of the dye solution, suggesting that the treatment was highly efficient. The efficiency of the photocatalyst was confirmed using XRD, SEM, and EPR techniques. The post-treatment product was characterized using FT-IR, HPLC, and GC-MS techniques. This helped us identify intermediate compounds and propose a pathway for the degradation of the dye.

REFERENCES

1. M. Sleiman, D. Vildozo, C. Ferronato and J. M. Chovelon, *Appl. Catal. B: Environ.*, **77**, 1 (2007).
2. V. Shah and D. Madamwar, *Int. Biodeter. Biodegr.*, **79**, 1 (2013).
3. M. Nakanishi, C. Yatome, N. Ishida and Y. Kitade, *J. Biol. Chem.*, **276**, 46394 (2001).
4. B. Bonakdarpour, I. Vyrides and D. C. Stuckey, *Int. Biodeter. Biodegr.*, **65**, 591 (2011).
5. Md. Milon Hossain, Md. Iqbal Mahmud, Md. Shohan Parvez, and H. M. Cho, *Environ. Eng. Res.*, **18**(3), 157 (2013).
6. P. A. Deshpande, S. Polisetti and G. Madras, *Langmuir*, **27**, 3578 (2011).
7. S. Suarez, J. Lema and F. Omil, *Bioresour. Technol.*, **100**, 2138 (2009).
8. R. A. Damodar, S. J. You and S. H. Ou, *Sep. Purif. Technol.*, **76**, 64 (2010).
9. E.-S. Z. El-Ashtoukhy, N. K. Amin and O. Abdelwahab, *Chem. Eng. J.*, **146**, 205 (2009).
10. C. A. Martinez-Huitle and E. Brillas, *Appl. Catal. B-Environ.*, **87**, 105 (2009).
11. A. Pirkarami, M. E. Olya and N, Y-Limaee, *Org Coat.*, **76**, 682 (2013).
12. S. H. Lin and C. C. Lo, *Environ. Technol.*, **17**, 841 (1996).
13. W.-J. Lau and A. F. Ismail, *Desalination.*, **245**, 321 (2009).
14. Y. Khambhaty, K. Mody, S. Basha and B. Jha, *Chem. Eng. J.*, **145**, 489 (2009).
15. M. A. Behnajady, N. Modirshahla, S. B. Tabrizi and S. Molanee, *J. Hazard. Mater.*, **152**, 381 (2008).
16. X. Wang, J. Wang, P. Guo, W. Guo and C. Wang, *J. Hazard. Mater.*,

169, 486 (2009).
17. S. Kitano, K. Hashimoto and H. Kominami, *Chem. Lett*., **39**, 627 (2010).
18. X. Li, T. Zhang, S. Gu, S.-Z. Kang, G. Li and J. Mu, *Sep. Purif. Technol.*, **108**, 139 (2013).
19. X. Jiang, L. Yang, P. Liu, X. Li and J. Shen, *Colloids Surf., B.*, **79**, 69 (2010).
20. M. Aliabadi and T. Sagharigar, *J. Appl. Environ. Biol. Sci*., **12**, 620 (2011).
21. X. Chen and S. S. Mao, *Chem. Rev.*, **107**, 2891 (2007).
22. B. Subash, B. Krishnakumar, R. Velmurugan and M. Swaminathan, *Sep. Purif. Technol*., **101**, 98 (2012).
23. J. Li, L. Li, L. Zheng, Y. Xian and L. Jin, *Electrochim. Acta*, **51**, 4942 (2006).
24. R. K. Sharma, S. Gulati, A. Pandey and A. Adholeya, *Appl. Catal. B-Environ*., **125**, 247 (2012).
25. R. Dastjerdi, M. R. M. Mojtahedi and A. M. Shoshtari, *J. Text I*, **101**, 204 (2010).
26. A. R. Quinlan and I. M. Hall, *Bioinformatics*., **26**, 841 (2010).
27. K. Tanaka and K. S. N. *Appl. Catal. B*., **39**, 305 (2002).
28. B. B. Yu, J. B. Zeng, L. F. Gong, M. S. Zhang, L. M. Zhang and X. Chen, *Talanta*., **72**, 1667 (2007).
29. W.-Y. Wang, M.-L. Yang and Y. Ku, *Chem. Eng. J*., **165**, 273 (2010).
30. J. Li, L. Zheng, L. Li, Y. Xian and L. Jin, *J. Hazard. Mater*., **139**, 72 (2007).
31. L. G. Devi, B. Nagaraj and K. E. Rajashekhar, *Chem. Eng. J*., **181-182**, 259 (2012).
32. W. Lina, H. Chenga, J. Minga, Y. Yua and F. Zhaoa, *J. Catal*., **291**, 149 (2012).
33. J. C. Colmenares, A. Magdziarz, K. Kurzydlowski J. Grzonka. O. Chernyayeva and D. Lisovytskiy, *Appl. Catal. B-Environ*., **134-135**, 136 (2013).
34. Y. Zhang and Q. Li, *Solid State Sci*., **16**, 16 (2013).
35. M. Y. Ghaly, J. Y. Farah and A. M. Fathy, *Desalination*, **2**, 74 (2007).
36. J. Saien and A. R. Soleymani, *J. Hazard. Mater*., **144**, 506 (2007).
37. G. Zhang, W. Choi, S. H. Kim and S. B. Hong, *J. Hazard. Mater*., **188**, 198 (2011).
38. R. Vyas, S. Sharma, P. Gupta, Y. K. Vijay, A. K. Prasad, A. K. Tyagi, K. Sachdev and S. K. Sharma, *J. Alloy Compd*., **554**, 59 (2013).
39. J. Araña, C. Fernández Rodríguez, O. González Díaz, J. A. Herrera Melián and J. Pérez Peña, *Catal. Today*, **101**, 261 (2005).
40. J. Araña, C. Garriga i Cabo, J. M. Doña-Rodríguez, O. González-Díaz, J. A. Herrera-Melián and J. Pérez-Peña, *Appl. Surf. Sci*., **329**, 60 (2004).
41. J. P. Espinós, J. Marales, A. Barranco, A. Caballero, J. P. Holgado and A. R. González-Elipe, *J. Phys. Chem. B*., **106**, 6921 (2002).
42. D. Robert, B. Dongui and J. V. Weber, *J. Photochem. Photobiol. A*, **156**, 195 (2003).
43. W. Chu, W. K. Choy and T. Y. So, *J. Hazard. Mater*., **141**, 86 (2007).
44. I. R. Guimarães, A. Giroto, L. C. A. Oliveira, M. C. Guerreiro, D. Q. Lima and J. D. Fabris, *Appl. Catal. B*., **91**, 581 (2009).
45. H. Chun, T. Yuchao and T. Hongxiao, *Catal. Today*, **90**, 325 (2004).
46. S. Guerrero, I. Guzman, G. Aguila, B. Chornik and P. Araya, *Appl. Catal. A-Gen*., **123-124**, 282 (2012).
47. A. Di Paola, E. García-López, G. Marcì, C. Martín, L. Palmisano, V. Rives and A. M. Venezia, *Appl. Catal. B: Environ*., **48**, 223 (2004).
48. I.-H. Tseng, J. C. S. Wu and H.-Y. Chou, *J. Catal*., **221**, 432 (2004).
49. C. He, Y. Xiong and X. Zhu, *Catal. Commun*., **4**, 183 (2003).
50. K. Chiang, R. Amal and T. Tran, *Adv. Environ. Res*., **6**, 471 (2002).
51. A. Di Paola, E. García-López, S. Ikeda, G. Marcì, B. Ohtani and L. Palmisano, *Catal. Today*, **75**, 87 (2002).
52. H. W. P. Carvalho, A. P. L. Batista, P. Hammer and T. C. Ramalho, *J. Hazard. Mater*., **184**, 273 (2010).
53. F. Boccuzzi, E. Guglielminotti, G. Martra and G. Cerrato. *J. Catal*., **146**, 449 (1994).
54. P. Larsson, A. Andersson, L. Wallenberg and B. Svensson, *J. Catal*., **163**, 279 (1996).
55. S. P. Xu and D. D. Sun, *Int. J. Hydrog. Energy*, **34**, 6096 (2009).
56. S. Xu, J. Ng, X. Zhang, H. Bai and D. D. Sun, *Int. J. Hydrog. Energy*, **35**, 5254 (2010).
57. S. S. Lee, H. Bai, Z. Liu and D. D. Sun, *Water Res*., **47**, 4059 (2013).
58. S. Rani, S. C. Roy, M. Paulose, O. K. Varghese, G. K. Mor, S. Kim, S. Yoriya, T. J. LaTempa and C. A. Grimes, *Phys. Chem. Chem. Phys*., **12**, 2780 (2010).
59. R. Asahi, T. Ohwaki, K. Aoki and Y. Taga, *Science*, **293**, 269 (2001).
60. R. Trejo-Tzab, J. J. Alvarado-Gil, P. Quintana and Bartolo-Pérez, *Catal. Today*, **193**, 179 (2012).
61. O. Diwald, T. L. Thompson, E. G. Goralski, S. D. Walck and J. T. Yates Jr., *J. Phys. Chem. B*., **108**, 52 (2004).
62. Y. Wang, C. X. Feng, Z. S. Jin, J. W. Zhang, J. J. Yang and S. L. Zhang, *J. Mol. Catal. A: Chem*., **260**, 1 (2006).
63. A. Ghicov, J. M. Macak, H. Tsuchiya, J. Kunze, V. Haeublein, S. Kleber and P. Schmuki, *Chem. Phys. Lett*., **419**, 426 (2006).
64. J. J. Xu, Y. H. Ao, M. D. Chen and D. G. Fu, *Appl. Surf. Sci*., **256**, 4397 (2010).
65. Z. Q. Liu, Y. C. Wang, W. Chu, Z. H. Li and C. C. Ge, *J. Alloys Compd*., **501**, 54 (2010).
66. J. Ananpattarachai, P. Kajitvichyanukul and S. Seraphin, *J. Hazard. Mater*., **168**, 253 (2009).
67. H. J. Liu, G. G. Liu and X. Y. Shi, *Colloid Surf. A*., **363**, 35 (2010).
68. M. Pourmand and N. Taghavinia, *Mater. Chem. Phys*., **107**, 449 (2008).
69. R. S. Sonawane, B. B. Kale and M. K. Dongare, *Mater. Chem. Phys*., **85**, 52 (2004).
70. Y. K. Chae, S. Mori and M. Suzuki, *Thin Solid Films*, **517**, 4260 (2009).
71. C.-M. Huang, L.-C. Chen, K.-W. Cheng and G.-T. Pan, *J. Mol. Catal. A: Chem*., **261**, 218 (2007).
72. N. Daneshvar, D. Salari and A. R. Khataee, *J. Photochem. Photobiol. A*., **162**, 317 (2004).
73. M. E. Olya, A. Pirkarami, M. Soleimani and M. Bahmaei, *J. Environ. Manage*., **121**, 210 (2013).
74. J. A. Navio, G. Colon and M. J. J. Trillas, *Appl. Catal. B: Environ*., **16**, 187 (1998).
75. S. B. Botta, J. A. Navio, M. C. Hidalgo and G. M. Restrepo, *J. Photochem. Photobiol. A: Chem*., **129**, 89 (1999).
76. M. Arami, N. Y. Livnaer, N. M. Mahamodi and N. S. Tabrizi, *J. Colloid Interface Sci*., **288**, 371 (2005).
77. C. Namasivayam and S. Sumithra, *J. Environ. Manage*., **74**, 207 (2005).
78. M. Valnice, B. Zanoni and J. Sene, *J. Photochem. Photobiol. A: Chem*.,

157, 55 (2003).
79. J. Shang, Y. Ch. Zhang, T. Zhu, Q. Wang and H. Song, *A: Catal. B: Environ.*, **102**(3-4), 464 (2011).
80. J. Wang, Y. Guo, B. Liu, X. Jin, L. Liu, R. Xu, Y. Kong and B. Wang, *Ultrason. Sonochem.*, **18**, 177 (2011).
81. A. W. Burton, K. Ong, T. Rea and I. Y. Chan, *Micropor. Mesopor. Mater.*, **117**, 75 (2009).
82. A. Manivel, S. Naveenraj, S. Kumar, P. Selvam and S. Anandan, *Sci. Adv. Mater.*, **2**, 51 (2010).
83. A. L. Attwood, D. M. Murphy, J. L. Edwards, T. A. Egerton and R. W. Harrison, *Res. Chem. Intermed.*, **29**, 449 (2003).
84. S. V. Chong, J. Xia, N. Suresh, K. Yamaki and K. Kadowaki, *Solid State Commun.*, **148**, 345 (2008).
85. J. Soria, J. Sanz, I. Sobrados, J. M. Coronado, F. Fresno and M. D. Hernandez-Alonso, *Catal. Today*, **129**, 240 (2007).
86. Y. Yamamotoa, S. Moribe, T. Ikpma, K. Akiyama, Q. Zhang, F. Saito and S. Tero Kubota, *Mol. Phys.*, **104**, 1733 (2006).
87. C. DiValentin, G. Pacchioni and A. Selloni, *Chem. Mater.*, **17**, 6656 (2006).
88. C. Chen, X. Sun, X. Jiang, D. Niu, A. Yu, Z. Liu and J. Li, *Nan. Res. Lett.*, **4**, 971 (2009).
89. G. He, W. Liu, X. Sun, Q. Chen, X. Wang and H. Chen, *Mater. Res. Bull.*, **48**, 1885 (2013).
90. V. Chandra, J. Park, Y. Chun, J. W. Lee, I. C. Hwang and K. S. Kim, *ACS Nano*, **4**, 3979 (2010).
91. X. F. Gao, H. B. Li, W. T. Sun, Q. Chen, F. Q. Tang and L. M. Peng, *J. Phys. Chem., C*, **113**, 7531 (2009).
92. H. Zhang, X. Quan, S. Chen, H. Yu and N. Ma, *Chem. Mater.*, **21**, 3090 (2009).
93. Q. Kang, Q. Z. Lu, S. H. Liu, L. X. Yang, L. F. Wen, S. L. Luo and Q. Y. Cai, *Biomaterials*, **31**, 3317 (2010).